

LES of Normally Impinging Elliptic Air-Jet Heat Transfer at $Re = 4400$

Yongping Li¹, Qizhao Lin¹ and Zuojin Zhu^{2,*}

¹ Department of Thermal Science and Energy Engineering, University of Science and Technology of China, Hefei, Anhui 230026, China

² Faculty of Engineering Science, University of Science and Technology of China, Hefei, Anhui 230026, China

Received 30 April 2015; Accepted (in revised version) 9 May 2016

Abstract. Jet impingement induced heat transfer is an important issue in engineering science. This paper presents results of large eddy simulation (LES) of normally impinging elliptic air-jet heat transfer at a Reynolds number of 4400, with orifice-to-plate distance fixed to be 5 in the unit of jet nozzle effective diameter D ($=\sqrt{ab}$). The elliptic aspect ratio (a/b) is $3/2$. While the target wall is heated under some condition of constant heat flux. The LES are carried out using dynamic subgrid model and OpenFOAM. The distributions of mean velocity components, velocity fluctuations, and subgrid stresses in vertical and radial directions, and the Nusselt numbers involving heat transfer through the target wall are discussed. The comparison with existing experimental and numerical results shows good agreement.

AMS subject classifications: 65C, 76F, 80A

Key words: Large eddy simulation, impinging air-jet, orifice-to-plate distance, subgrid heat flux, elliptic aspect ratio.

1 Introduction

Jet impingement is a conventional method to enhance heat transfer [1, 2]. Increasing the normal velocity gradient and turbulence intensity of fluid flow near the impingement surface can improve the heat transfer [3]. Impinging jet with heat transfer has become an ad hoc problem in engineering science due to its great significance in applications. Before introducing the main objective of this paper, a research background of impinging jet flows, including experimental work [3–24] and numerical simulations [25–55] is presented below.

*Corresponding author.

Email: zuojin@ustc.edu.cn (Z. J. Zhu)

Elliptic jets have decided advantages for technological applications over circular jets as reported by Hussain et al. [7]. To explore advantages achieved by jet forcing due to self-excitation, using hot-wire measurements and flow visualization, Hussain et al. [7] have studied an elliptic whistler (i.e., self-excited) air jet of 2/1 aspect ratio which, in contrast to an elliptic jet issuing from a contoured nozzle, displays no axis switching, but significantly increased spread in the major-axis plane. They found that its near-field mass entrainment is considerably higher (by as much as 70%) than that of a non-whistling jet. Unexpected dynamics of the elliptic vortical structures in the whistler jet compared to that in the non-whistling jet. Vortices rolled up from the lip of the elliptic pipe impinge onto the collar, producing secondary vortices; interaction of these two opposite-signed vortices is shown to cause the different behaviour of the whistler jet.

The mixing due to a heated elliptic air-jet was measured by Zhang and Chua [12]. They measured velocity and temperature for a contoured contraction nozzle elliptic air jet with a 2/1 aspect ratio issuing into stagnant unconfined surroundings, with hot-wire and cold-wire anemometers. The experimental results suggest that the use of heated elliptic jets could offer enhanced mixing performance in relevant applications.

Many numerical studies have been carried out by means of direct numerical simulation (DNS), Reynolds averaged Navier-Stokes (RANS) modelling, and large eddy simulation (LES). To predict turbulent impinging circular jets whose orifice-to-plate distance in the unit of jet-nozzle diameter (H/D) was fixed at 2, and 6, the jet issuing Reynolds number was fixed at 2.3×10^4 and 7×10^4 , with an extended version of the finite-volume code TEAM based on RANS modelling, Craft et al. [25] obtained numerical results of the impinging jet and compared with experimental data of Baughn and Shimizu [5], Cooper et al. [6]. After predicting heat transfer due to circular jet impingement, Park and Sung [26] reported that their nonlinear low-Reynolds-number $k-\varepsilon$ model is generally satisfactory, in this model the limiting near-wall behavior and nonlinear Reynolds stress representations are incorporated.

Zuckerman and Lior [27] conducted RANS modelling of impinging jet heat transfer, in which the selected model equations, the quantitative assessments of model errors, and the judgments of model suitability were provided. To explore the heat and fluid flow performance of deflector under periodic jet impingement, using the RNG $k-\varepsilon$ model [35], Zhang et al. [34] have recently found that temperature variation of heat resistance layer in deflector occurs stable periodic fluctuations after four impingement periods; the temperature of the impinged wall surface increases with the decrease of jet distance or the increase of horizontal angle.

LES results of a forced semi-confined impinging circular jet were reported by Olssen and Fuchs [37]. The Reynolds number was 10^4 , and the inflow was forced at a Strouhal number of 0.27. The orifice-to-plate distance in the unit of jet-nozzle diameter H/D was set as 4. By studying the mean velocity, the turbulence statistics, the subgrid scale (SGS)-model effects, the dynamic behavior of the jet with a focus on the near wall region, they confirmed that the existence of separation vortices in the wall jet region, and revealed that these secondary vortices are related to the radially deflected primary vortices generated

by the circular shear layer of the jet, the primary vortex structures that reach the wall were helical and non axi-symmetrical.

LES results of impinging circular air-jet heat transfer were reported by Hällqvist [42]. The LES model was a basic one without explicit subgrid-scale (SGS) modeling and without explicit filtering. Instead, the numerical scheme was used to account for the necessary amount of dissipation. By using the computational grid as a filter, the cutoff wave number depends explicitly on the grid spacing. The grid is staggered and constructed in a Cartesian coordinate system. To explain how the dynamics of the flow and heat transfer are affected, a great variety of inlet conditions were considered. Hällqvist revealed that the top-hat and the turbulent inflow conditions yield a higher rate of incoherent small scale structures. The applied level of swirl at the velocity inlet also has significant influence on the rate of heat transfer. The turbulence level increases with swirl, which is positive for heat transfer, and so also the spreading of the jet.

LES of a normally impinging circular jet issuing from a long pipe at a Reynolds number $Re = 2 \times 10^4$, and $H/D = 2$ were done by Hadžiabdic and Hanjalic [46]. They pointed out that care must be taken in interpreting LES results in impinging flows. There are interesting time and spatial dynamics of the vorticity and eddy structures and their imprints on the target wall, characterized by tilting and breaking of the edge ring vortices before impingement, flapping, precessing, splitting and pairing of the stagnation point/line, local unsteady separation and flow reversal at the onset of radial jet spreading, streaks pairing and branching in the near-wall region of the radial jets, and others. Their LES results can also provide a basis for plausible explanations of some of the experimentally detected statistically-averaged flow features such as double peaks in the Nusselt number and the negative production of turbulence energy in stagnation region.

LES of the formation of nano-particles in an impinging twin jet was encompassed by Yin and Lin [43]. The results show that the nucleation produces a large number of nanoparticles, and gas-to-nanoparticle conversion mostly takes place in the interface region of the two jets, the circumambience of the jets, and region near the plane. Increasing the distance from nozzle to plane is beneficial to the reduction of nanoparticle formation. While the LES of impinging transverse jet in the near-wall zone was done by Fan, Zhang, and Wang [44]. The LES results reproduced the skewed jet shear layer vortices close to the jet nozzle and the scarf vortex in the near-wall zone, in good agreement with the experimental observations.

LES of turbulent circular jets normally impinging on a target surface were carried out by Uddin et al. [47], with the focus on the case of a jet which issues from a circular pipe into stagnant surrounding at a relatively high value of jet-issuing Reynolds number (2.3×10^4) for which experimental data are available. The LES work of Uddin et al. is aimed to obtain the details of the mean flows and the turbulence fields including distributions of all components of the turbulent heat fluxes. The LES results were used to assess three alternative models for the turbulent heat fluxes which differ from the conventional Fourier's Law by not being based on the assumption of proportionality between the eddy and thermal diffusivities via a constant Prandtl number. They found that only one of the

models considered succeeds in representing the effects on the heat fluxes of the complex strain field associated with the stagnation region and the subsequent development into the wall jet region, and discussed the relevant reasons for this outcome.

In the LES of Nicoud and Toda et al. [49], singular values were used to build a SGS model. They found that the so-called σ -model has a low computational cost, is easy to implement, and does not require any homogeneous direction in space or time. The results obtained with the proposed model are systematically equivalent or slightly better than the results from the dynamic Smagorinsky model [50].

For the recent development of computation of impinging jet heat transfer, a review has been presented by Dewan et al. [52]. They reviewed the effects of different SGS models, boundary conditions, numerical schemes, grid distribution, and size of the computational domain adopted in various LES of this impinging jet, together with a review of DNS of the same geometry and computation of other complex impinging flows, and a description of some recent attempts in RANS modelling of impinging flows. It was concluded with a listing of some important findings and future directions in the computation of impinging jet flows.

More recently, Toda, Cabrit et al. [53] have conducted a LES-dedicated prediction of a pulsatile hot-jet impinging a flat-plate in the presence of a cold turbulent cross-flow. Two eddy-viscosity-based SGS models are studied: the σ -model [49] and the dynamic Smagorinsky model [50], indicating that both models give similar results during the first phase of the experiment. However, the dynamic Smagorinsky model could not accurately predict the vortex-ring propagation, while the σ -model provides a better agreement in comparison with the experimental data.

Dairay et al. [54] have conducted a LES of turbulent jet impinging on a heated wall using high-order numerical schemes, and compared the LES results with DNS and experimental data, indicating that highly accurate numerical methods can lead to correct predictions of velocity statistics and heat transfer but only if a procedure is used to regularize the large-scale dynamics computed explicitly.

Most of the investigations as mentioned above are involving circular jet, while the work of impinging elliptic jet heat transfer is less studied. The objective of this LES is to explore the heat and fluid flow characteristics of impinging elliptic air-jet at a Reynolds numbers of 4400 and a fixed orifice-to-plate distance ($H/D = 5$) with OpenFOAM for elliptic aspect ratio (a/b) fixed at $3/2$. Therefore, the distributions of velocity components, their fluctuations, and the mean Nusselt numbers, as well as the relevant comparisons with existing experimental and numerical results are reported and discussed in the Section 4.

2 Governing equations

The impinging elliptic air-jet heat transfer problem, as schematically shown in Fig. 1, involves an elliptic air-jet of aspect ratio $3/2$ impinging normally to a flat plate, with

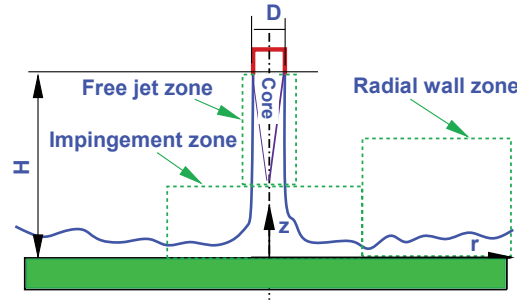


Figure 1: Schematic of normally impinging elliptic air-jet.

a fixed orifice-to-plate distance of $H/D = 5$. The jet air temperature is assumed to be the same as the ambient temperature, but lower than that of the plate surface heated by constant heat flux, implying that the round air jet just plays a cooling role on the target wall. The jet Reynolds number defined by $Re = W_b D / \nu$ is 4400, implying the impinging air-jet is turbulent [47]. The flow is assumed to be incompressible, and cooling mode is mainly related to forced convection, while the contributions due to buoyancy caused natural convection and wall thermal radiation are assumed to be negligible. Following the numerical work [27, 47], the governing equations for the air-jet heat transfer problem are given by

$$\frac{\partial \hat{u}_i}{\partial x_i} = 0, \tag{2.1a}$$

$$\frac{\partial \hat{u}_i}{\partial t} + \frac{\partial(\hat{u}_j \hat{u}_i)}{\partial x_j} = -\frac{1}{\rho} \frac{\partial \hat{p}}{\partial x_i} + \nu \frac{\partial}{\partial x_j} \left[\frac{\partial \hat{u}_i}{\partial x_j} + \frac{\partial \hat{u}_j}{\partial x_i} \right] - \frac{1}{\rho} \frac{\partial \tau_{ij}^s}{\partial x_j}, \tag{2.1b}$$

$$\frac{\partial(c_p \hat{T})}{\partial t} + \frac{\partial(c_p \hat{u}_j \hat{T})}{\partial x_j} = \frac{1}{\rho} \frac{\partial}{\partial x_j} \left[\Gamma c_p \frac{\partial \hat{T}}{\partial x_j} \right] - \frac{1}{\rho} \frac{\partial q_j^s}{\partial x_j}, \tag{2.1c}$$

where \hat{u}_i is the velocity component in the x_i direction, ρ , \hat{T} and \hat{p} are the fluid density, temperature, and pressure respectively, the over hat $\hat{}$ denotes the resolved variables. The subgrid scale stress is defined by

$$\tau_{ij}^s = \rho(\widehat{u_i u_j} - \hat{u}_i \hat{u}_j). \tag{2.2}$$

The subgrid scale (SGS) model for closure of momentum equations is based on a gradient-diffusion hypothesis, which is given by a relation between anisotropic stress and (large-scale) strain rate tensor

$$\tau_{ij}^s - \frac{1}{3} \delta_{ij} \tau_{kk}^s = 2\rho \nu_s \left(\hat{S}_{ij} - \frac{1}{3} \delta_{ij} \hat{S}_{kk} \right), \tag{2.3}$$

where ν_s is the subgrid viscosity, given by

$$\nu_s = (c_s \Delta)^2 \hat{S} = (c_s \Delta)^2 \sqrt{2 \hat{S}_{ij} \hat{S}_{ij}}, \tag{2.4}$$

Table 1: Thermophysical properties of air used in the LES.

$\rho(\text{kg/m}^3)$	$c_p(\text{kJ/kg}\cdot\text{K})$	$k(\text{W/m}\cdot\text{K})$	$\nu(\text{m}^2/\text{s})$	Pr
1.1767	1.0066	0.0262	1.58×10^{-5}	0.7196

where

$$\widehat{S}_{ij} = \frac{1}{2} \left(\frac{\partial \widehat{u}_i}{\partial x_j} + \frac{\partial \widehat{u}_j}{\partial x_i} \right) \quad (2.5)$$

is the resolved strain rate. In Eq. (2.4), Δ is the grid filter width, c_s is a constant specified by the dynamic Smagorisky model (DSM) [57].

The subgrid heat flux q_j^s is expressed as

$$q_j^s = \rho c_p (\widehat{u}_j \widehat{T} - \widehat{u}_j \widehat{T}). \quad (2.6)$$

Again, using gradient diffusion assumption similar to Uddin et al. [47], let Pr_s be subgrid Prandtl number, we have

$$q_j^s = -\frac{\rho \nu_s}{Pr_s} c_p \frac{\partial \widehat{T}}{\partial x_j}, \quad (2.7)$$

where $(\rho \nu_s / Pr_s)$ denotes the subgrid thermal diffusivity. In the present LES, the subgrid Prandtl number Pr_s is set at 0.85. It is noted that Pr_s can also be dynamically adjusted for the consideration of backscatter effect. But for the LES of impinging jet, it can be assumed to be a constant value around 0.9, as reported by Uddin [48].

The top and side boundaries of the computational domain are assigned to have constant pressure conditions, the so called open boundary condition allows the occurrence of possible reverse flow. The inflow turbulence intensity is assumed at the level of 1%, so that the root mean square (rms) value of velocity fluctuation for each component can be set as one percent of the jet issuing velocity W_b . On the surface of target plate wall, no-slip condition and constant heat flux condition are used. The heat flux is set at 1000W/m^2 . While the ambient air temperature in this LES was set as 300K, at which thermo-physical properties under standard atmospheric condition are given in Table 1.

3 Numerical method

An unstructured grid system is used in the LES by virtue of control-volume approach. In the discretization of governing equations (2.1a)-(2.1c), second order Crank-Nicolson method is used in the treatment of the temporal gradient term, while the second order central-difference scheme is used in the treatment of the spatial gradients in the nonlinear convective terms. The algebraic equations are solved by PISO algorithm.

Computational domain of the LES is an elliptical cylinder. Time step (Δt) in OpenFOAM is self-adjusted by setting a condition that the Courant number should be less than 0.5, i.e., $\Delta t |U| / \delta x < 0.5$, where δx refers to the cell size in the direction of the velocity,

Table 2: Jet-issuing velocity and normalized finest grid distance in the three cases.

Re	W_b (m/s)	z^+	t_0 (s)	$\bar{\tau}$	$N_c^{1/3}$	R_s^\dagger
4400	9.93	≤ 1.31	7.0493×10^{-3}	580.63	107.298	1.833

and $|U|$ refers to the magnitude of the velocity through that cell. While the normalized finest grid distance close to the target wall ($z^+ = zu_\tau/\nu$, u_τ refers to the friction velocity) can be as small as 1.31 for $Re = 4400$, causing the time step sometimes at the level of micro-second. With the total control-volume number $N_c = 1235494$, and the value of t_0 shown in Table 2, assuming the average time step is $5\mu s$, i.e., $\Delta\bar{t} \approx 5\mu s/t_0 = 7.0929 \times 10^{-4}$, we can estimate the ratio of maximal allowable number of time steps for the problem and the actual number of time steps used to obtain the result, $R_s = 1.833$ for $S^{\max} \approx 0.3\%$, as shown in Table 2. The ratio R_s was predicted by means of the approach described in the recent numerical study of Smirnov, et al. [58], involving hydrogen fuel rocket engines simulation using LOGOS simulator [59]. This approach can be used for estimating the accumulated error in numerical work based on Navier-Stokes equations. As reported in [58], the ratio R_s characterizes reliability of results to determine the limit of the simulations. Indirectly it characterizes the accumulated error. The higher the value R_s is, the lower is the error. On tending R_s to unity the error tends to maximal allowable value.

As the reliability of numerical results is evaluated by a step ratio approach [58], the relevant verification is done in comparison with measured empirical results, thus the checking of grid independence is omitted. The DSM-based LES results will be discussed in the next section.

4 Results and discussion

Let the effective diameter of elliptic jet-nozzle be $D (= \sqrt{ab})$, and the jet-issuing speed be W_b , if both are taken as the length and speed scales, the time scale t_0 is D/W_b . In the present LES, jet nozzle diameter D is fixed at 0.007m, jet issuing velocity (W_b) is fixed at 9.93m/s, then time scale (t_0), and time period used in the statistical analysis of LES results ($\bar{\tau}$) can be obtained, as shown in Table 2. Since the elliptic nozzle has an aspect ratio of $\lambda^2 = 3/2$, the elliptic long axis length (a) and elliptic short axis length (b) must be equal to λD and D/λ . For simplicity, we define the long and short axis by x and y , respectively.

The instantaneous streamlines and temperature contours in the plane of $y = 0$ are shown in Figs. 2(a)-(b), with part (a) corresponding to the top region $z \in (0.75, 5]$, with part (b) to the near wall region $z \in (0, 0.75]$. Here the partition value 0.75 is assigned with respect to the mean turbulent kinetic energy field shown in Fig. 8. As constant heat flux is used as heating mode of the target wall, air temperature in the near wall region are higher than that in the top region as shown in Fig. 2.

[†] $S^{\max} \approx 0.3\%$, for $\Delta\bar{t} = 7.0929 \times 10^{-4}$, the time steps $n \approx 818607$, when the final time is $\bar{\tau} = 580.63$.

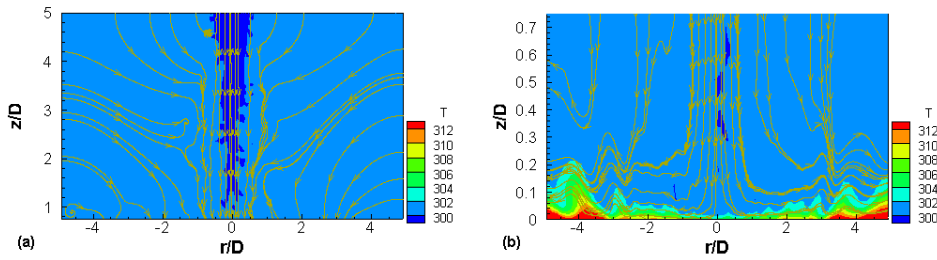


Figure 2: Instantaneous streamlines and temperature contours at $\bar{t} = 65.82$ in the plane of $y = 0$ in top region $z \in (0.75, 5]$ (a) and the near wall region $z \in (0, 0.75]$ (b).

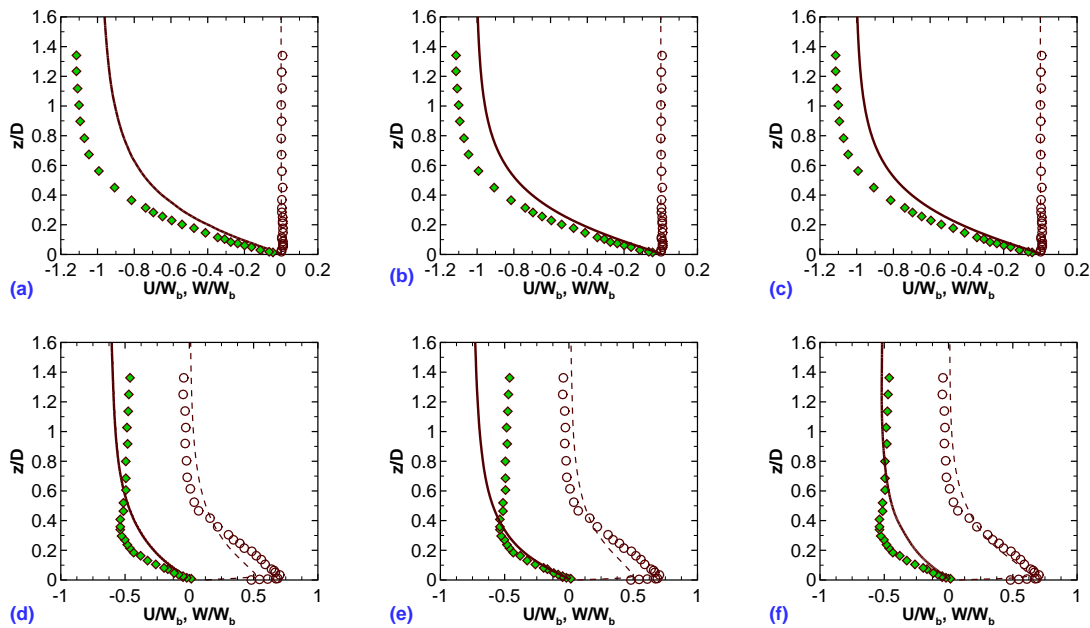


Figure 3: Comparison of velocity component in the z -direction, (a)-(c) at $r/D = 0, x/D = 0, y/D = 0$; (d)-(f) at $r/D = 0.5, x/D = 0.5, y/D = 0.5$. The data labeled by circle and diamond were from [8]; solid line denotes W/W_b ; dashed line represents U/W_b .

Comparisons of velocity components in the z -direction at six positions [$r/D = 0, x/D = 0, y/D = 0$ (a)-(c), and $r/D = 0.5, x/D = 0.5, y/D = 0.5$ (d)-(f)] are shown in Figs. 3(a)-(f), where the experimental data labeled by unfilled circle for U/W_b and green-filled diamond for W/W_b are obtained from [8]. The experimental data of Geers, Tummens and Hanjalic [8] are obtained in the case of $H/D = 2$ at $Re = 2.3 \times 10^4$. At the two radial positions, the calculated velocity distributions in the z -direction agree with the measured data favorably. The discrepancy is mainly caused by the different jet impinging conditions.

On the other hand, the comparison of mean velocity distributions in the r -direction with the LES results of Hadziabdic and Hanjalic [46] is shown in Figs. 4(a)-(f), with parts

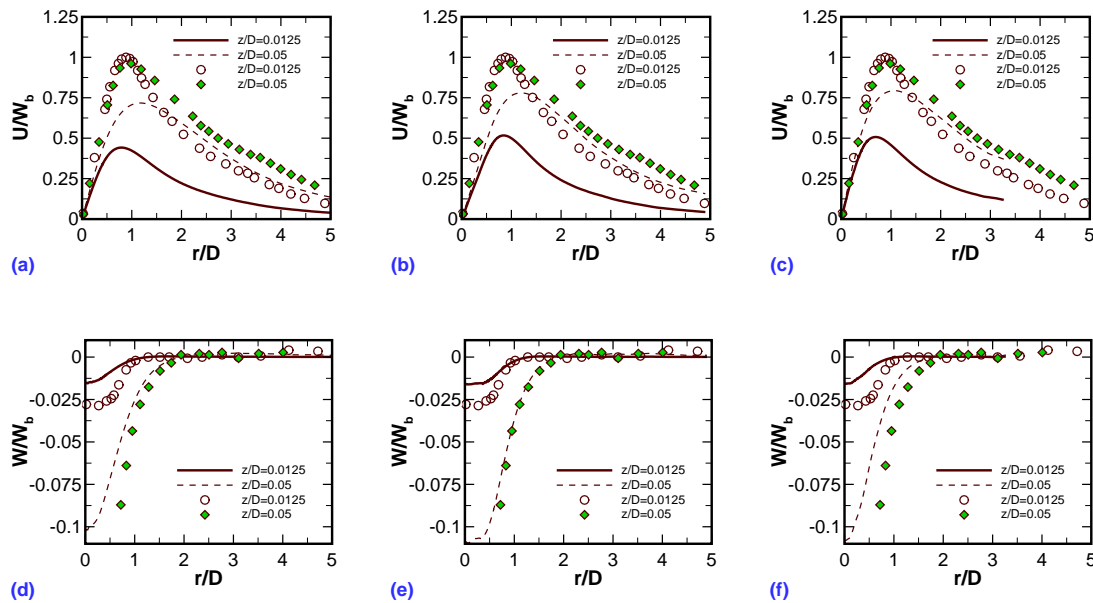


Figure 4: Comparison of mean velocity distributions in the r -direction, (a)-(c) for U/W_b , Round, ELA, and ESA; (d)-(f) for W/W_b , Round, ELA, and ESA. The data labeled by unfilled circle and green-filled diamond were abstracted from the numerical work [46].

(a)-(c) showing the mean velocity component U/W_b at two distances to the wall surface $z/D = 0.0125, 0.05$, and parts (d)-(f) showing W/W_b at the two distances. In Figs. 4(a)-(c), it can be seen that the radial velocity distribution is sensitive to the wall distance z/D . The value of mean velocity U/W_b is larger at $z/D = 0.05$ as compared with that at $z/D = 0.0125$, with the velocity difference at the two z/D positions being dependent of r/D . In Figs. 4(d)-(f), it is seen that a quite good agreement with the LES results as reported in [46], an observable discrepancy appears only in the stagnation point region $r/D \in (0, 1)$. Similarly, the discrepancy can be attributed to the different condition of jet impingement.

For the normally impinging elliptic air-jet heat transfer, the velocity components given in parts (b)-(c), (e)-(f) are calculated without circumferential (θ -) averaging, which has been used for parts (a) and (d). Hence, in the caption of Fig. 4, the elliptic-long axis (ELA) and elliptic-short axis (ESA) are addressed to indicate that the velocity distribution curves are calculated merely using time average and axis-symmetrical assumption. This simplicity treatment of LES data is also used for the predictions of velocity fluctuations and subgrid stresses in the case of elliptic air-jet impingement, as shown in Figs. 5-6.

It is noted that the orifice-to-plate distance in the present LES is larger than existing experimental and LES studies [8, 46] with a multiplicative factor of about 2.5, the jet issuing Reynolds number is smaller than the existing results used in comparison with a

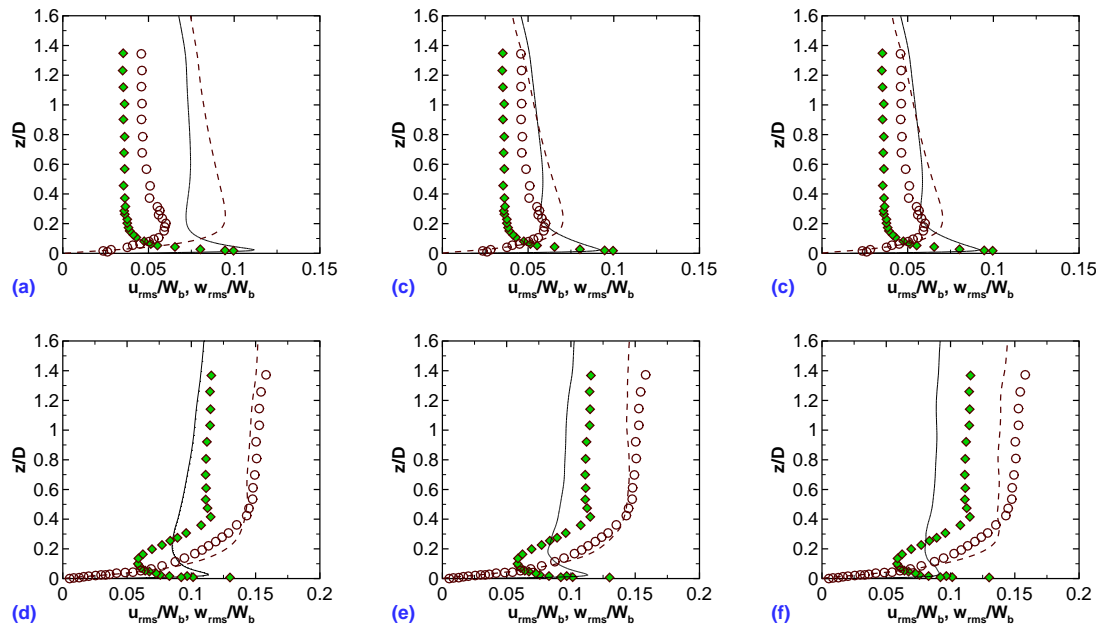


Figure 5: Comparison of velocity fluctuations in the z -direction, (a)-(c) at $r/D=0$, $x/D=0$, and $y/D=0$; (d)-(f) at $r/D=0.5$, $x/D=0.5$ and $y/D=0.5$. The data labeled by circle and diamond were abstracted from [8], solid line denotes u_{rms}/W_b , dashed line represents w_{rms}/W_b .

factor of about 0.2, and the jet nozzle has changed to elliptic type with an aspect of 3/2. All these features, can bring about the discrepancies of root mean square values of velocities and the different distributions of subgrid stresses in the r -directions, as can be seen from Figs. 5-6.

For round air-jet heat transfer, the target surface is described in polar coordinates. Averaging the heat transfer coefficient of jet impingement in the θ -direction from zero to 2π , the heat transfer coefficient h should be a single function of r . Further averaging the local Nusselt number

$$Nu = hD/k \tag{4.1}$$

in the r -direction, the mean Nusselt number can be expressed as

$$Nu_{av} = \frac{2}{r^2} \int_0^r Nu \cdot \eta d\eta. \tag{4.2}$$

However, for normally impinging elliptic air-jet heat transfer, to see the performance of elliptically issuing more directly, the θ - averaging is not used, the r - average is alternated by x - and y - average. Fig. 7 shows the distributions of local Nusselt number in the r -direction, where the unfilled small brown circle symbols labeled by ELA are corresponding to elliptic-long-axis, the unfilled small blue triangle symbols labeled by ESA are relevant to elliptic-short-axis, the black curve labeled by Round refers to the case of

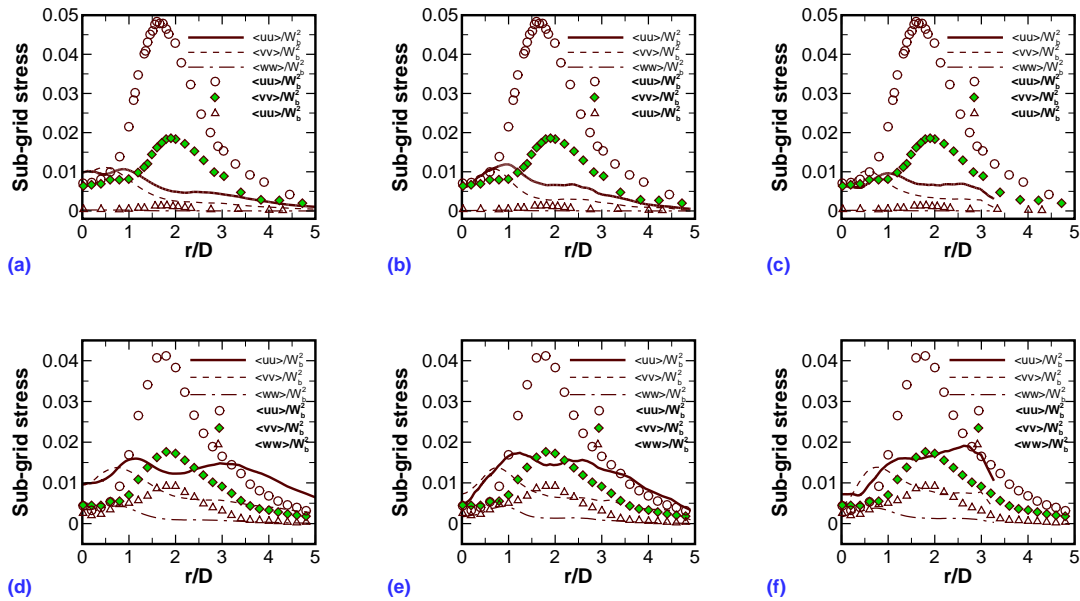


Figure 6: Comparison of subgrid stress in the r -direction (a)-(c) at $z/D = 0.0125$, Round, ELA, and ESA; (d)-(f) at $z/D = 0.05$, Round, ELA, and ESA. The data labeled by unfilled circle and green-filled diamond were abstracted from the numerical work [46].

round air-jet as reported in [56]. The local Nusselt number along the ELA differs from that along the ESA. Along the ELA, the local Nusselt number has a second peak, and a higher value in the range of $r/D \in (0.5, 2)$.

To demonstrate the reason, the contours of mean turbulent kinetic energy (TKEmean) are given in Fig. 8, which are labeled by 0.05, 0.1, 0.5, 1, 1.5, 2, 2.5, and 3 in the unit of kinetic energy per unit mass. The TKEmean is calculated by

$$\overline{\text{TKE}} = \frac{1}{2} \overline{u_i'^2}, \tag{4.3}$$

where u_i' ($= \hat{u}_i - \overline{\hat{u}_i}$) is the instantaneous fluctuation of velocity component in the x_i -direction, with the over-line denoting time average. Fig. 8 indicates that the change of nozzle cross section can lead to TKEmean pattern in the $y = 0$ plane has large differences in comparison with that in the x -plane. To some extent, the TKEmean pattern has indicated some turbulent properties of elliptic air-jet impingement. In addition to reflect the wall jet structure, Fig. 8 also shows that in the near wall region the TKEmean has values in the range of $\overline{\text{TKE}} \in (0.05, 2.5)$. But in the jet core, the TKEmean is less than 0.05, in the top region outside of the jet core, there are some zones where the TKEmean can be larger than 2.5.

As shown in Fig. 9, the predicted mean Nusselt number agrees with the data abstracted from [4] satisfactorily. It can be seen that for the given jet-issuing $\text{Re} = 4400$, the

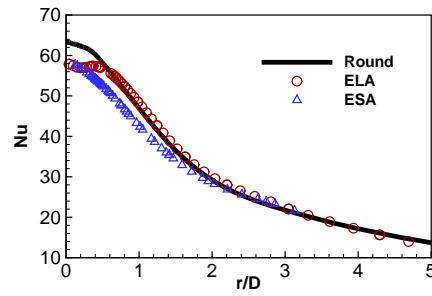


Figure 7: Distributions of local Nusselt numbers in the r -direction.

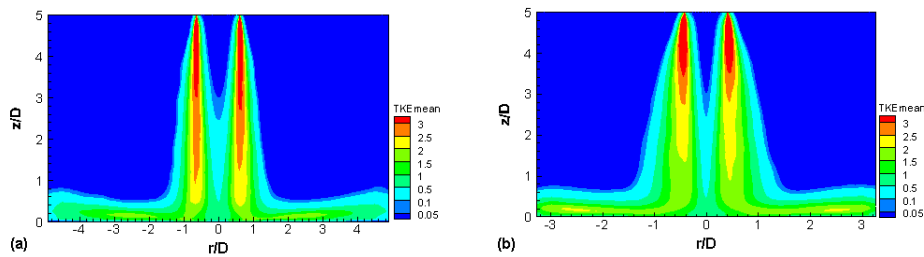


Figure 8: Contours of mean turbulent kinetic energy in the plane of (a) $y=0$, and (b) $x=0$.

normal impingement of elliptical air-jet results in a slightly lower value of mean Nusselt number in stagnation region as compared with that predicted in the case of round air-jet [56], indicating that the change of nozzle cross section from round to elliptic can slightly weakened heat transfer rate in stagnation region, the nozzle shape change has resulted in the corresponding change of jet core shape, jet impinging form, and turbulent flow structure on the target plate. It is noted that for $r/D \geq 2.5$, the data were calculated by empirical expression [4]

$$Nu_{av,exp} = F \cdot [1.36Re^{0.574}Pr^{0.42}], \tag{4.4}$$

where the multiplicative factor

$$F = [D/r(1 - 1.1D/r)] / [1 + 0.1D/r(H/D - 6)] \tag{4.5}$$

is a function of D/r and H/D . The expression Eq. (4.4) is valid merely for the Reynolds number range of $Re \in (2000, 30000)$.

While for $r/D < 2.5$ in the region close to the stagnation point, the experimental data are obtained with respect to some measured curves [4]. The favorable comparison of heat transfer indicates that software OpenFOAM is applicable in predicting normally impinging air-jet heat transfer at the moderate Reynolds number.

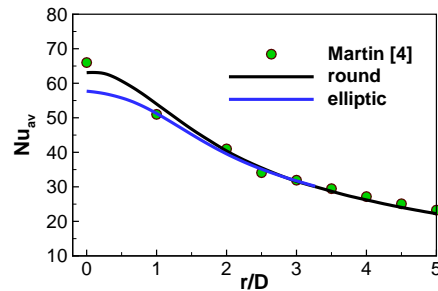


Figure 9: Comparison of distributions of mean Nusselt number.

5 Conclusions

For the heat transfer problem of normally impinging elliptic air-jet of aspect ratio 3/2 at a jet Reynolds number of 4400 with orifice-to-plate distance fixed at five jet-nozzle diameters, LES were conducted to obtain the primary findings are listed below:

1. The predicted mean Nusselt number has satisfactory consistency with measured empirical results, indicating the software OpenFOAM does have potential in predicting some thermal engineering problems.
2. The change of nozzle cross section change from round to elliptic can decrease mean heat transfer rate mainly in stagnation region. The local Nusselt number along elliptic-long axis has a second peak value, while along elliptic-short axis, it decreases monotonically along the r -direction; in some radial range, for a given r -value, it has a lower value as compared with that predicted along the elliptic-long axis.
3. For vertical and radial distributions of flow variables such as mean velocity components, velocity fluctuations and subgrid stresses, the discrepancies in comparison with existing LES results are mainly caused by different jet impinging conditions. The patterns of TKEmean in the vertical planes respectively containing the short and short axes have large differences.

Acknowledgments

This research was financially supported by National Science and Technology Ministry with Project No. 2013BAK03B08 and NSFC (51376171).

References

- [1] K. JAMBUNATHAN, E. LAI, M. A. MOSS AND B. L. BUTTON, *A review of heat transfer data for single circular jet impingement*, Int. J. Heat Fluid Flow, 13 (1992), pp. 106–115.

- [2] R. VISKANTA, *Heat transfer to impinging isothermal gas and flame jets*, Exp. Thermal Fluid Sci., 6 (1993), pp. 111–134.
- [3] K. ICHIMIYA AND Y. YOSHIDA, *Oscillation effect of impingement surface on two-dimensional impingement heat transfer* ASME J. Heat Transfer, 131 (2009), 011701.
- [4] H. MARTIN, *Heat and mass transfer between impinging gas jets and solid surfaces*, in: James PH (Eds), *Advances in Heat Transfer*, Elsevier, New York, 1977, pp. 1–60.
- [5] J. W. BAUGHN AND S. SHIMIZU, *Heat transfer measurements from a surface with uniform heat flux and an impinging jet*, ASME J. Heat Transfer, 111(4) (1989), pp. 1096–1098.
- [6] D. COOPER, D. C. JACKSON, B. E. LAUNDER AND G. X. LIAO, *Impinging jet studies for turbulence model assessment: I. Flow-field experiments*, Int. J. Heat Mass Transfer, 36(10) (1993), pp. 2675–2684.
- [7] H. S. HUSSAIN AND F. HUSSAIN, *The elliptic whistler jet*, J. Fluid Mech., 397 (1999), pp. 23–44.
- [8] L. F. G. GEERS, M. J. TUMMERS AND K. HANJALIC, *Experimental investigation of impinging jet arrays*, Exp. Fluids, 36 (2004), pp. 946–958.
- [9] C. G. LI AND J. M. ZHOU, *Experimental and numerical simulation study of heat transfer due to confined impinging circular jet*, Chem. Eng. Technol., 30(10) (2007), pp. 1355–1361.
- [10] O. VIPAT, S. S. FENG, T. KIM, A. M. PRADEEP AND T. J. LU, *Asymmetric entrainment effect on the local surface temperature of a flat plate heated by an obliquely impinging two-dimensional jet*, Int. J. Heat Mass Transfer, 52 (2009), pp. 5250–5257.
- [11] H. Q. YANG, T. KIM, T. J. LU AND K. ICHIMIYA, *Flow structure, wall pressure and heat transfer characteristics of impinging annular jet with/without steady swirling*, Int. J. Heat Mass Transfer, 53 (2010), pp. 4092–4100.
- [12] Z. K. ZHANG AND L. P. CHUA, *Mixing due to a heated elliptic air jet*, Int. J. Heat Mass Transfer, 55 (2012), pp. 4566–4579.
- [13] Y. XU, L. H. FENG AND J. J. WANG, *Experimental investigation of a synthetic jet impinging on a fixed wall*, Exp. Fluids, 54 (2013), 1512.
- [14] Y. F. XING AND B. WEIGAND, *Optimum jet-to-plate spacing of inline impingement heat transfer for different crossflow schemes*, ASME J. Heat Transfer, 135 (2013), 072201.
- [15] J. Z. ZHANG, S. GAO AND X. M. TAN, *Convective heat transfer on a flat plate subjected to normally synthetic jet and horizontally forced flow*, Int. J. Heat Mass Transfer, 57 (2013), pp. 321–330.
- [16] Y. H. XIE, P. LI, J. B. LAN AND D. ZHANG, *Flow and heat transfer characteristics of single jet impinging on dimpled surface*, ASME: J. Heat Transfer, 135 (2013), 052201.
- [17] D. ZHANG, H. C. QU, J. B. LAN, J. H. CHEN AND Y. H. XIE, *Flow and heat transfer characteristics of single jet impinging on protrusioned surface*, Int. J. Heat Mass Transfer, 58 (2013), pp. 18–28.
- [18] C. KANG AND H. X. LIU, *Turbulent features in the coherent central region of a plane water jet issuing into quiescent air*, ASME J. Fluids Eng., 136 (2014), 081205.
- [19] Y. Z. YU, J. Z. ZHANG AND H. S. XU, *Convective heat transfer by a row of confined air jets from round holes equipped with triangular tabs*, Int. J. Heat Mass Transfer, 72 (2014), pp. 222–233.
- [20] S. S. FENG, J. J. KUANG, T. WEN, T. J. LU AND K. ICHIMIYA, *An experimental and numerical study of finned metal foam heat sinks under impinging air jet cooling*, Int. J. Heat Mass Transfer, 77 (2014), pp. 1063–1074.
- [21] K. WANG, H. W. LI AND J. Q. ZHU, *Experimental study of heat transfer characteristic on jet impingement cooling with film extraction flow*, Appl. Thermal Eng., 70 (2014), pp. 620–629.
- [22] X. L. WANG, H. B. YAN, T. J. LU, S. J. SONG AND T. KIM, *Heat transfer characteristics of an inclined impinging jet on a curved surface in crossflow*, ASME J. Heat Transfer, 136 (2014),

- 081702.
- [23] C. J. ZHANG, G. Q. XU, H. W. LI, J. N. SUN AND N. CAI, *The effect of weak crossflow on the heat transfer characteristics of short-distance impinging cooling*, ASME J. Heat Transfer, 136 (2014), 112201.
- [24] Y. Z. YU, J. Z. ZHANG AND Y. SHAN, *Convective heat transfer of a row of air jets impingement excited by triangular tabs in a confined crossflow channel*, Int. J. Heat Mass Transfer, 80 (2015), pp. 126–138.
- [25] T. J. CRAFT, L. GRAHAM AND B. E. LAUNDER, *Impinging jet studies for turbulence model assessment II. An examination of the performance of four turbulence models*, Int. J. Heat Mass Transfer, 36(10) (1993), pp. 2685–2697.
- [26] T. S. PARK AND H. J. SUNG, *Development of a near-wall turbulence model and application to jet impingement heat transfer*, Int. J. Heat Fluid Flow, 22(1) (2001), pp. 10–18.
- [27] N. ZUCKERMAN AND N. LIOR, *Jet impingement heat transfer: physics, correlations, and numerical modeling*, Adv. Heat Transfer, 39 (2006), pp. 565–631.
- [28] M. Z. YU, L. H. CHEN, H. H. JIN AND J. R. FAN, *Large eddy simulation of coherent structure of impinging jet*, J. Thermal Sci., 14(2) (2005), pp. 150–155.
- [29] S. RHEA, M. BINI, M. FAIRWEATHER AND W. P. JONES, *RANS modelling and LES of a single-phase, impinging plane jet*, Comput. Chem. Eng., 33(8) (2009), pp. 1344–1353.
- [30] R. DUTTA, A. DEWAN AND B. SRINIVASAN, *Comparison of various integration to wall (ITW) RANS models for predicting turbulent slot jet impingement heat transfer*, Int. J. Heat Mass Transfer, 65 (2013), pp. 750–764.
- [31] Y. Q. ZU, Y. Y. YAN AND J. MALTSON, *Numerical study on stagnation point heat transfer by jet impingement in a confined narrow gap*, ASME J. Heat Transfer, 131 (2009), 094504.
- [32] P. XU, B. M. YU, S. X. QIU, H. J. POH AND A. S. MUJUMDAR, *Turbulent impinging jet heat transfer enhancement due to intermittent pulsation*, Int. J. Thermal Sci., 49 (2010), pp. 1247–1252.
- [33] Z. LIU AND Z. P. FENG, *Numerical simulation on the effect of jet nozzle position on impingement cooling of gas turbine blade leading edge*, Int. J. Heat Mass Transfer, 54 (2011), pp. 4949–4959.
- [34] J. J. ZHANG, Y. P. XIONG, Z. G. QU AND W. Q. TAO, *Numerical study of flow and heat transfer performance of deflector under periodic jet impingement*, J. Eng. Thermophys., 35(7) (2014), pp. 1395–1400.
- [35] V. YALHOT AND S. A. ORSZAG, *Renormalization group analysis of turbulence: I. basic theory*, J. Sci. Comput., 1 (1986), pp. 1–51.
- [36] P. WANG, J. Z. LV, M. L. BAI, Y. Y. WANG AND C. Z. HU, *Numerical investigation of the flow and heat behaviours of an impinging jet*, Int. J. Comput. Fluid Dyn., 28(6-10) (2014), pp. 301–315.
- [37] M. OLSSON AND L. FUCHS, *Large eddy simulations of a forced semiconfined circular impinging jet*, Phys. Fluids, 10(2) (1998), pp. 476–486.
- [38] P. R. VOKE AND S. GAO, *Numerical study of heat transfer from an impinging jet*, Int. J. Heat Mass Transfer, 41(4-5) (1998), pp. 671–680.
- [39] T. CZIESLA, G. BISWAS, H. CHATTOPADHYAY AND N. K. MITRA, *Large-eddy simulation of flow and heat transfer in an impinging slot jet*, Int. J. Heat Fluid Flow, 22(5) (2001), pp. 500–508.
- [40] M. TSUBOKURA, T. KOBAYASHI, N. TANIGUCHI AND W. P. JONES, *A numerical study on the eddy structures of impinging jets excited at the inlet*, Int. J. Heat Fluid Flow, 24(4) (2003), pp. 500–511.
- [41] F. BEAUBERT AND S. VIAZZO, *Large eddy simulations of plane turbulent impinging jets at moderate Reynolds numbers*, Int. J. Heat Fluid Flow, 24(4) (2003), pp. 512–519.
- [42] T. HÄLLQVIST, *Large eddy simulation of impinging jets with heat transfer*, Technical Reports from Royal Institute of Technology, Department of Mechanics, 2006, S-100 44 Stockholm,

Sweden.

- [43] Z. Q. YIN AND J. Z. LIN, *Numerical simulation of the formation of nanoparticles in an impinging twin-jet*, J. Hydrodyn. Ser. B, 19(5) (2007), pp. 533–541.
- [44] J. Y. FAN, Y. ZHANG AND D. Z. WANG, *Large-eddy simulation of three dimensional vortical structures for an impinging transverse jet in the near region*, J. Hydrodyn. Ser. B, 19(3) (2007), pp. 314–321.
- [45] M. POPOVAC AND K. HANJALIC, *Large-eddy simulations of flow over a jet-impinged wall-mounted cube in a cross stream*, Int. J. Heat Fluid Flow, 28 (2007), pp. 1360–1378.
- [46] M. HADŽIABDIC AND K. HANJALIC, *Vortical structures and heat transfer in a round impinging jet*, J. Fluid Mech., 596 (2008), pp. 221–260.
- [47] N. UDDIN, S. O. NEUMANN, B. WEIGAND AND B. A. YOUNIS, *Large-eddy simulations and heat-flux modeling in a turbulent impinging jet*, Numer. Heat Transfer Part A, 55 (2009), pp. 906–930.
- [48] N. UDDIN, *Turbulence Modelling of Complex Flows in CFD*, Institute of Aerospace Thermodynamics, Universität Stuttgart, Ph.D Thesis, (2008), pp. 41–43.
- [49] F. NICOUD, H. B. TODA, O. CABRIT, S. BOSE AND J. LEE, *Using singular values to build a subgrid-scale model for large eddy simulations*, Phys. Fluids, 23 (2014), 085106.
- [50] M. GERMANO, U. PIOMELLI, P. MOIN AND W. CABOT, *A dynamic subgrid-scale eddy viscosity model*, Phys. Fluids A, 3(7) (1991), pp. 1760–1765.
- [51] G. LODATO, L. VERVISCH AND P. DOMINGO, *A compressible wall-adapting similarity mixed model for large-eddy simulation of the impinging round jet*, Phys. Fluids, 21 (2009), 0351023.
- [52] A. DEWAN, R. DUTTA AND B. SRINIVASAN, *Recent trends in computation of turbulent jet impingement heat transfer*, Heat Transfer Eng., 33(4-5) (2012), pp. 447–460.
- [53] H. B. TODA, O. CABRIT, K. TRUFFIN, G. BRUNEAUX AND F. NICOUD, *Assessment of subgrid-scale models with a large-eddy simulation-dedicated experimental database: The pulsatile impinging jet in turbulent cross-flow*, Phys. Fluids, 26 (2014), 075108.
- [54] T. DAIRAY, V. FORTUN, E. LAMBALLAIS AND L. E. BRIZZI, *LES of a turbulent jet impinging on a heated wall using high-order numerical schemes*, Int. J. Heat Fluid Flow 50 (2014), pp. 177–187.
- [55] W. WU AND U. PIOMELLI, *Large-eddy simulation of impinging jets with embedded azimuthal vortices*, J. Turbulence, 16(1) (2015), pp. 44–66.
- [56] Y. P. LI, Q. Z. LIN, T. H. YE AND Z. J. ZHU, *Large eddy simulation of a normally impinging round air jet with heat transfer at a Reynolds number of 4400*, in: Proceeding of Mechanical and Civil Engineering, ICMCE2612, December 13-14, 2014, Wuhan, China.
- [57] U. PIOMELLI AND J. H. LIU, *Large-eddy simulation of rotating channel flows using a localized dynamic-model*, Phys. Fluids, 7(4) (1995), pp. 839–848.
- [58] N. N. SMIRNOV, V. B. BETELIN, R. M. SHAGALIEV, V. F. NIKITIN, I. M. BELYAKOV, YU. N. DERYUGUIN, S. V. AKSENOV AND D. A. KORCHAZHKIN, *Hydrogen fuel rocket engines simulation using LOGOS code*, Int. J. Hydrogen Energy, 39 (2014), pp. 10748–10756.
- [59] V. B. BETELIN, R. M. SHAGALIEV, S. V. AKSENOV, I. M. BELYAKOV, YU. N. DERYUGUIN, D. A. KORCHAZHKIN, A. S. KOZELKOV, V. F. NIKITIN, A. V. SARAZOV AND D. K. ZELENSKIY, *Mathematical simulation of hydrogen-Coxygen combustion in rocket engines using LOGOS code*, Acta Astronautica, 96 (2014), pp. 53–64.